RSC Advances

PAPER

View Article Online
View Journal | View Issue

Cite this: *RSC Adv.*, 2018, **8**, 16171

Characterization of three-point bending properties of metal–resin interpenetrating phase composites

Bibo Yao,[ab] Zhaoyao Zhou, *[a] Liuyang Duan[a] and Zengtao Chen[b]

Metal–resin composites provide improved combinations of mechanical properties of raw materials. A novel metal–resin interpenetrating phase composite (IPCs) has been fabricated by spontaneously infiltrating unsaturated polyester resin into porous short-fiber preforms under vacuum conditions. In this study, three-point bending experiments are performed to characterize the bending properties of the IPCs. The fractographs after bending are examined to distinguish their characteristics. The flexural strength increases almost linearly from 42 ± 4 MPa to 119 ± 5 MPa in the in-plane direction and 59 ± 4 MPa to 151 ± 8 MPa in the through-thickness direction with an increasing fiber fraction ranging from 16.78 vol% to 32.11 vol%. The structures and bending properties of the IPCs exhibit significant anisotropy. Compared with the in-plane direction, higher bending strength and flexural modulus with smaller displacement at maximum bending force are observed in the through-thickness direction. The finer fibers contribute to improving the flexural strength (from 76 ± 6 MPa to 98 ± 5 MPa for the IPCs with about 23 vol% fiber fraction from 160 μm to 90 μm fiber diameters in the in-plane directions) and modulus. The fracture of the IPC after bending presents different appearances in different directions and the anisotropy becomes less severe with decreasing fiber fraction. Resin fracture, fiber necking and fracture, and debonding are the main fracture mechanisms.

Received 6th March 2018
Accepted 25th April 2018

DOI: 10.1039/c8ra01953c

rsc.li/rsc-advances

Introduction

Weight reduction and superior mechanical properties are demanded in the development and practical applications of many novel materials.[1,2] The interpenetrating phase composite (IPC) is a new type of composite structure with three-dimensional interconnectivity of both phases, which makes them markedly different from traditional composites whose discrete, dispersed and isolated reinforcement phases are imbedded in matrix phases, such as fibers, whiskers, or particles.[1,3,4] The properties of traditional composites are usually dominated by the continuous matrix material with limited contribution from the disperse phase.[2] However, the unique structure of IPC might improve the elastic and yield properties relative to traditional composites and have good transmission of stresses between phases.[5–7] Each phase can contribute its most desirable attributes for its contiguous morphology. The nature of the fiber, matrix, and interface properties determine the properties of the composites.[8]

Numerous IPCs have been investigated in the literature, and ceramic–polymer,[3,9] ceramic–metal,[10–14] metal–metal[4,15,16] and polymer–polymer[17–19] IPCs are some types of main interest. Konopka *et al.*[9] fabricated novel ceramic–polymer composites *via* infiltration of porous SiO_2 by polynitrile-urea-urethane elastomer and found that the composites exhibited a high compression strength together with ability to sustain large deformations. Spontaneously infiltrating the metal into the ceramic preform was impossible without reactive systems under carefully controlled conditions for the bad wetting nature of most metal melts on ceramic substrates.[7,20,21] Graphite/aluminum composites with an interpenetrating network microstructure were produced by indirect squeeze casting process, and the results revealed that both flexural strength and fracture toughness for IPC were increased by 200% for the un infiltrated material at room temperature.[12] Yu *et al.*[22] pointed out that the presences of SiC particles in Zn22Al/10 vol% SiCp composite foams altered the deformation mechanism of ZA22 foams. Zhou *et al.*[15] demonstrated that the compressive properties of the 304 stainless steel fiber/ZA8 zinc alloy IPCs can be improved after casting both in room and high temperatures. Jena *et al.*[18] developed a novel polymer–polymer IPC by mixing tetrafunctional epoxy resin (TGDDM) with diallyl bisphenol A (DBA) modified bismaleimide (BMI). They demonstrated that compared to neat epoxy resin, the mechanical properties such as tensile, flexural and impact strength were improved by 25%, 30% and 45%, respectively after incorporating of DBA modified BMI into the epoxy resin enhanced. Al-Ketan *et al.*[19] investigated uniaxial compression properties of polymer–polymer, two-

[a]*National Engineering Research Center of Near-Net-Shape Forming for Metallic Materials, School of Mechanical and Automotive Engineering, South China University of Technology, Guangzhou 510640, People's Republic of China. E-mail: zhyzhou@scut.edu.cn*

[b]*Department of Mechanical Engineering, University of Alberta, Edmonton, AB T6G1H9, Canada*

phase IPCs fabricated by Polyjet 3D printing technology. They pointed out that the hard phase carried a larger fraction of the load, and the softer phase confined cracks and prevented catastrophic failure.

One important kind of the IPCs is metal–polymer IPCs. They can synthesize the properties of components, *i.e.*, one phase can offer good toughness and thermal conductivity, while the other phase enhances stiffness and dielectric properties to form the synergistical structural.[23] Recently, metal–polymer IPCs have received significant attentions.[1,24,25] The three dimensional microstructure is difficult to control and characterize in the process of producing IPCs. Current research mainly focuses on metal foam–polymer IPCs. However, it is expensive to fabricate metal foams. Thus it is necessary to find an economic method to produce those IPCs. The metal preforms produced by compacting and solid-sintering short fibers are considered as an economic technology in fabricating IPCs. In addition, unsaturated polyester resin (UP) is widely used in IPCs for its outstanding properties.[26]

Our previous work has reported a new metal–resin IPC and its tensile behavior.[5] In this work, a novel 304 stainless steel fiber/resin IPC was produced by infiltrating a type of unsaturated polyester resin into the preforms under vacuum conditions. The anisotropic microstructure and three point bending behavior were investigated. The fractographs were observed to determine the fracture characteristics of the IPC after bending process.

Material and methods

Manufacturing process of the metal–resin IPCs

The manufacturing process of the metal–resin IPCs can be described as two stages as our previous work:[5] porous preforms forming and vacuum infiltration.

The processing procedure of the porous preforms contains the following steps: fiber fabricating, mold pressing and vacuum sintering.[27] First, the short 304 stainless steel fibers ranging from 10 to 15 mm in length were fabricated by cutting stainless steel wires (0.8 and 1.5 mm in external diameter, 90 and 160 μm in fiber diameter, respectively) and the details were described in our previous work.[27] Then the short fibers were stochastically put into a designed mold followed with compaction and vacuum sintering at 1330 °C for 90 min. A stage heating method was used to optimize heating rates in the sintering process. The heating rate was 10 °C min^{-1} with the temperature below 800 °C and decreased to 6 °C min^{-1} with the temperature above 800 °C. The preforms were naturally cooled to room temperature in the furnace after finishing sintering. Quality-volume method[27] was used to calculate the average porosity P, so the average fiber volume fraction in the IPC is $1 - P$.

The vacuum impregnation process was conducted in the WHS-20 vacuum furnace. For every IPC sample, the infiltrant consists of 600 g unsaturated polyester resin (LH-6993), 5 g methyl ethyl ketone peroxide (LH-508) and 5 g promoters (LH-817) from Guangzhou Liheng Mekpo Technology co. Ltd. Unsaturated polyester resin was poured in a mold followed with methyl ethyl ketone peroxide. After they were sufficiently stirred, promoters were added and stirred to form the uniform mixture, *i.e.*, infiltrant. Then the preforms were put in the infiltrant and they were moved to the furnace to vacuumize for 2 hours to completely infiltrate. After that, the temperature was increased to 98 °C and held for 2 hours. On finishing this process, the IPC samples were naturally cooled to room temperature in the vacuum furnace. The schematic diagram of the manufacturing process and the IPC sample are shown in Fig. 1.

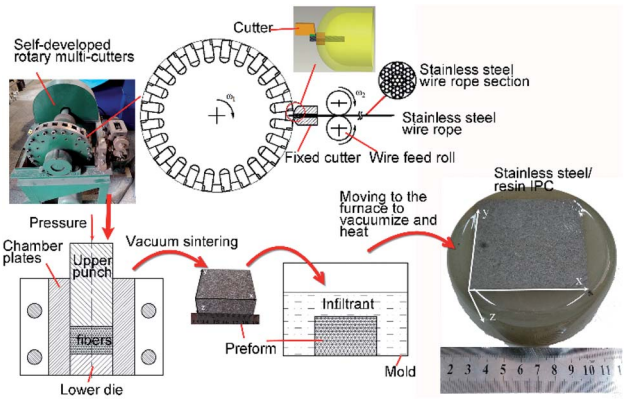

Fig. 1 The schematic diagram of the manufacturing process and the macroscopic appearance of metal/resin IPC.

Microstructure and three-point bending characterization of the IPCs

Our previous work demonstrated that the microstructure and tensile behavior of the metal/resin IPCs present anisotropy,[5,27] so the three-point bending behavior will also present anisotropy. The microscopic structures of the IPCs were observed by a scanning electron microscope (S-3700N, Japan) with high voltage of 20 kV under high vacuum mode. Specimens constructed from the different directions of the metal–resin IPCs were machined using milling for the microstructure observation and three-point bending tests. The specimen surfaces for microstructure observation were finished to a very high polish in several stages, beginning with coarse 180 grit emery paper, then with successively finer 400, 800 and 1200 grits, and finally plated with gold before observation. The geometry of specimen of three-bending tests was cuboid shape with dimensions of 50 mm in length, 10 mm in width, and 4 mm in height. The span of 40 mm between two supporters were selected in the three-point bending tests. All bending tests were conducted on an electronic, universal mechanical testing machine (AG-100NX, Japan) at a constant crosshead speed of 1 mm min^{-1}. All tests were conducted at room temperature (approximately 25 °C) for three specimens of each IPC group. During each test, the applied compression load and displacement were recorded continuously by the software. The fracture surfaces of the deformed specimens were plated with gold and then monitored by a scanning electron microscope (S-3700N, Japan) with high voltage of 20 kV under high vacuum mode.

In the three-point bending test, the maximum stress at the surface of sample was calculated by the following formula:[28]

$$\sigma_{bb} = \frac{F_{bb} L_s}{4W} \quad (1)$$

$$W = \frac{1}{6} bh^2 \quad (2)$$

$$E = \frac{L_s{}^3 \Delta F}{4bh^3 \Delta S} \quad (3)$$

where σ_{bb} is the flexural strength (MPa), F_{bb} is the maximum bending force (N), L_s is the span of two supports (mm), W stands for the cross section coefficient (mm^3), b is the width of IPC (mm), h is the height of IPC (mm), E is the flexural modulus (MPa), ΔF and ΔS are the increments of bending force and displacement in the initial linear bending force–displacement curve, respectively.

Results and discussion

Microstructural characterization of the stainless steel/resin IPC

The stainless steel fibers are distributed in the preforms randomly, and many sintering joints between the fibers are formed to produce a spatial intertexture structure from the surface to the center.[27] The special three dimensional structure and interconnected open pores are produced, providing the possibility of completely infiltrating the preform with infiltrant. The microstructures of the stainless steel/resin IPC in the in-plane (x–y plane) and through-thickness (x–z plane) directions are shown in Fig. 2a and b, respectively. The gray phase is resin and the lighter phase is 304 stainless steel fibers. It is clear that no evident voids present in the resin and interface, indicating good infiltration under the given process.[5] During the heating and isothermal holding process, free radical copolymerization reacts in cross-linked impregnant for consolidation to form the novel IPCs. Fig. 2 shows the anisotropic microstructure of the IPC in the two directions, *i.e.*, most fibers distributed in the IPC are parallel to the pressure face, namely the x–y plane. Many sintering joints are clear for material migration between fiber and fiber bundle interconnection points. It is noted that nonuniform fibers are distributed in the IPC for stochastically putting fibers into a mold and different compaction force extensions during the processing.

Bending fracture process of the IPC

The typical three-point bending force–displacement plots of the IPC with 160 μm fiber diameter and different fiber fractions in different directions are shown in Fig. 3. The in-plane direction in Fig. 3 refers to the compression loading direction along the x-direction or y-direction, which is parallel to the x–y surface. The through-thickness direction refers to the compression loading direction parallel to z-direction. From Fig. 3, it is easily found that the three-point bending fracture processes of the IPCs present the following three stages: elastic stage, plastic deformation stage after yielding, and fracture stage. The bending

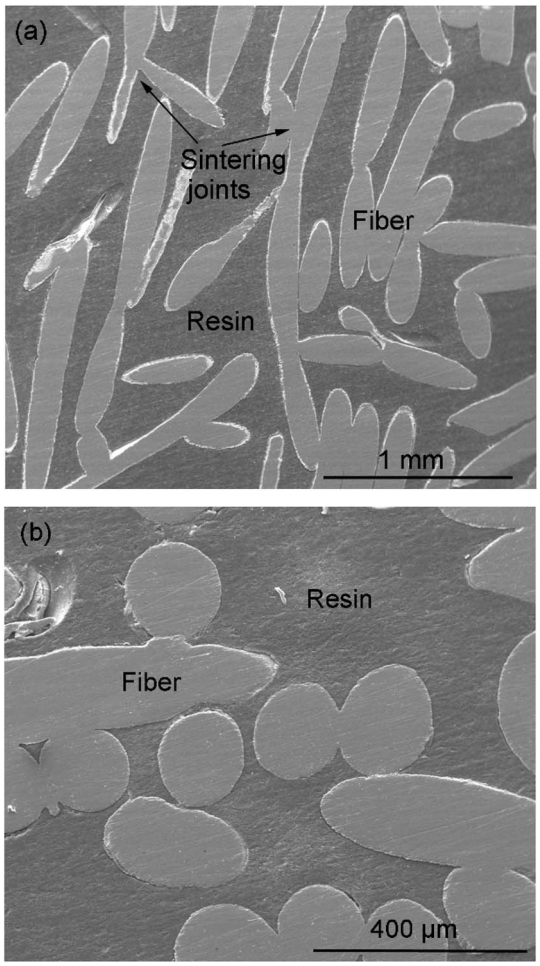

Fig. 2 SEM micrographs of the IPC with 32.11 vol% fiber fraction and 160 mm fiber diameter: (a) in-plane (x–y plane) direction and (b) through-thickness (x–z plane) direction.

processes initially exhibit short-term linear elastic deformation which is treated well by the isostrain rule of mixtures at the displacement below 0.5 mm when both phases are defoming elastically, and then enter nonlinear stages, in agreement with ref. 29 and 30. After elastic deformation, the deformation process quickly enters into yielding, and starts to deform plastically. The bending force gradually increases due to the plastic deformation of three dimensional reticulated structures and resins until it reaches its maximum value, and macro-cracks appear in the weaknesses of resin and interface at this process. After that, the bending force decreases dramatically with the increase of displacement for the expansion of cracks in samples and the IPCs finally reach complete destruction of the entire structure. After the maximum stress, the resin collapse and the fibers debond, so the fibers withstand the main stress until they fracture, while the resin contributes little to load bearing. Note that the yield stages are not obvious. It is noted that the IPCs present non-linear elastic behavior due to the elastic deformation of the stainless steel preform accompanied by a plastic deformation of the resin, similar to the mechanical process of metal–resin IPCs[5] and metal matrix IPCs.[15,30] The bending behavior exhibits obvious anisotropy. Compared with

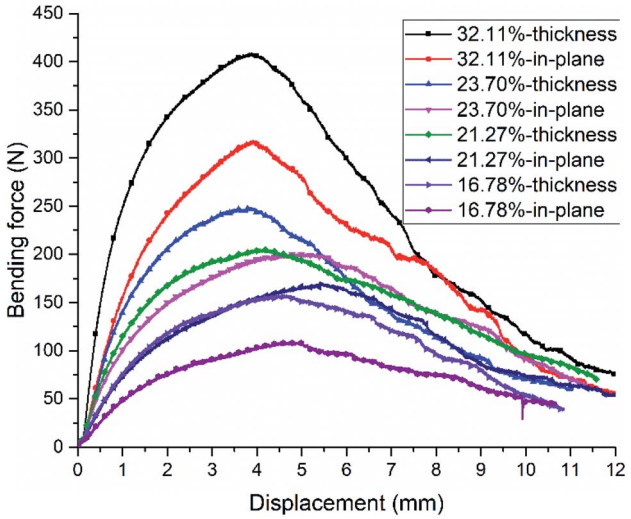

Fig. 3 Typical three-point bending force–displacement curves of with 160 μm fiber diameter and different fiber fractions in different directions.

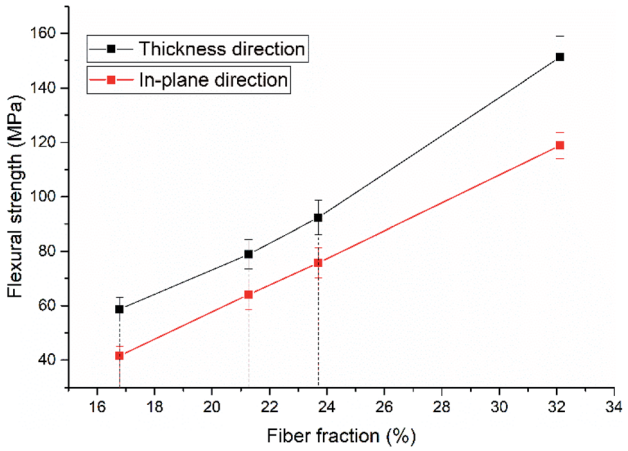

Fig. 4 The flexural strengths of the IPCs with 160 μm fiber diameter and different fiber fractions in different directions.

the through-thickness direction, the displacement at maximum bending force is slightly less than that of the IPC in in-plane direction, *i.e.*, 3.89–4.57 mm in through-thickness direction and 3.97–5.39 mm in in-plane direction. Due to the initial short-term linear elastic stage, the flexural modulus can be evaluated by the initial linear slopes of the load–displacement curves according to eqn (3).[2] It is demonstrated that the flexural modulus increases with increasing fiber fractions ranging from 16.78 vol% to 32.11 vol% in both directions[31] and is higher for the IPC in through-thickness direction, *i.e.*, 1414 ± 159 MPa to 5465 ± 533 MPa in in-plane direction and 2133 ± 273 MPa to 10 394 ± 915 MPa in through-thickness direction. In the same direction, the displacement at maximum bending force changes little with increasing fiber fraction, which is different from the results that increasing fiber fraction can improve the elongation at tensile stress of metal/resin IPC.[5]

Fig. 4 shows the flexural strength of the IPCs with 160 μm fiber diameter and different fiber fractions in different directions. It reveals that flexural strength increases nearly linearly with increasing fiber fraction ranging from 16.78 vol% to 32.11 vol% in both directions, *i.e.*, 42 ± 4 MPa to 119 ± 5 MPa in in-plane direction and 59 ± 4 MPa to 151 ± 8 MPa in through-thickness direction, in agreement with the results of ref. 31. After infiltrating of resin into the preforms, the flexural strength and modulus are significant improved.[31,32] There are many strengthening mechanism in composites, including stress transfer from the matrix to the reinforced phase, dislocation strengthening, refining grain size, *etc*[30]. Usually, the strengthening mechanisms differ for different composites and the first two factors mainly affect the properties in the process for the network structure of the IPC. Compared with the in-plane direction, the IPCs have a higher bending strength and flexural modulus in the through-thickness direction. The skeletons of the preforms in longitudinal section have more bending-torsion deformation, eventually improving the bending properties. In addition, the difference is more serious with the increasing fiber fraction. When the fiber fraction is 32.11 vol%, the flexural strength increases by 32 MPa (from 119 ± 5 MPa to 151 ± 8 MPa) from in-plane to through-thickness direction, which is about two times (from 42 ± 4 MPa to 59 ± 4 MPa) that of the IPC with 16.78 vol% fiber fraction.

Our previous work has demonstrated that finer fibers can significantly improve the tensile strength of metal/resin IPC[5] and compressive strength of the 304 stainless steel fiber/ZA8 IPC.[15] In this paper, the effect of fiber diameter on the flexural properties has also been investigated. Fig. 5 and 6 show the bending force–displacement curves in, and the flexural strength with different fiber diameters, respectively. It is clear that finer fibers can improve the flexural strength and modulus. In addition, they slightly enlarge the displacement at maximum bending force. From the IPC with 23.70 vol% fiber fraction and 160 μm fiber diameter to 23.17 vol% fiber fraction and 90 μm fiber diameter, the flexural strengths increase from 76 ± 6 MPa to 98 ± 5 MPa and flexural modulus increases from 3973 ± 414 MPa to 5266 ± 547 MPa. It is obvious that finer fibers can significantly improve the strength for more fibers and three-dimensional structures per unit volume participate in the

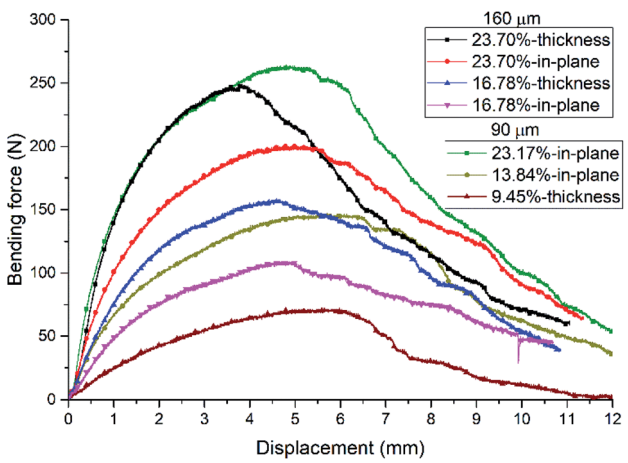

Fig. 5 Contrast bending force–displacement curves with different fiber diameters.

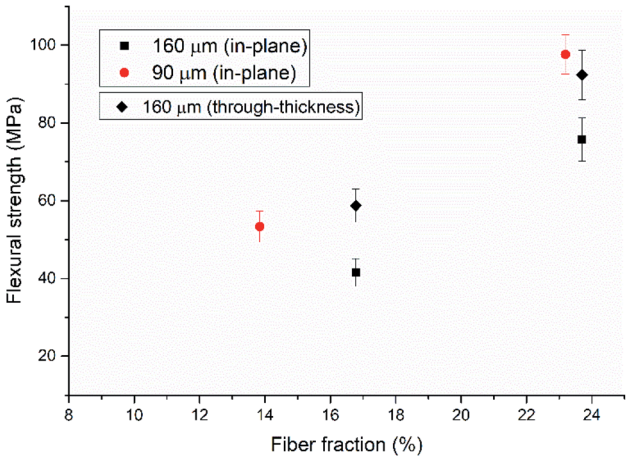

Fig. 6 Flexural strength with different fiber diameters and fractions.

bending process. For the same fiber fraction, finer fiber diameter results in the narrower pore distributes,[33] which contributes to toughness increase of IPC's.[31] From ref. 30, the stress transfer and dislocation strengthening may contribute more to improve flexural strength because more dislocation strengthening happens for the finer microstructure. The flexural strength of the metal–resin IPC with 9.45 vol% fiber fraction and 90 μm fiber diameter is 30 ± 3 MPa, which is slightly higher than that of unsaturated polyester resin, *i.e.*, 27.5 MPa.[34] So the flexural properties have little improvement after the fiber fraction lower than 9.45 vol%.

Bending fractographic examinations

The appearances of metal–resin IPCs with 23.17 vol% fiber fraction and 90 μm fiber diameter, and 13.84 vol% fiber fraction and 90 μm fiber diameter are shown in Fig. 7. By comparing the fracture surface, the difference is obvious in different direction when the fiber fraction is 23.17 vol% while the anisotropy is not obvious when the fiber fraction is less than 13.84 vol%. The cracks on the surface along the loading direction are irregular, and the fracture presents serration on the surface of the

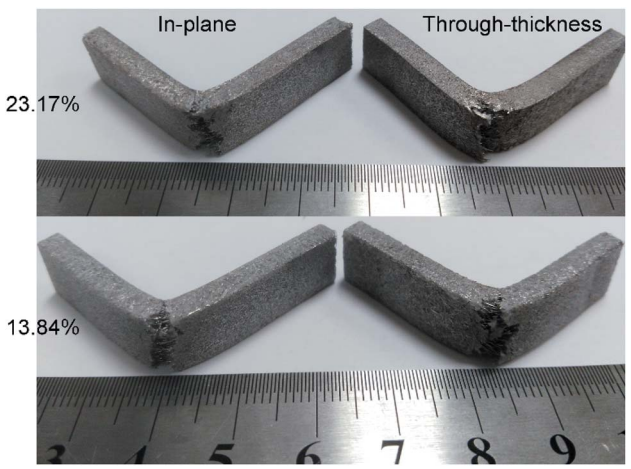

Fig. 7 The appearance of metal–resin IPCs with different fiber fractions.

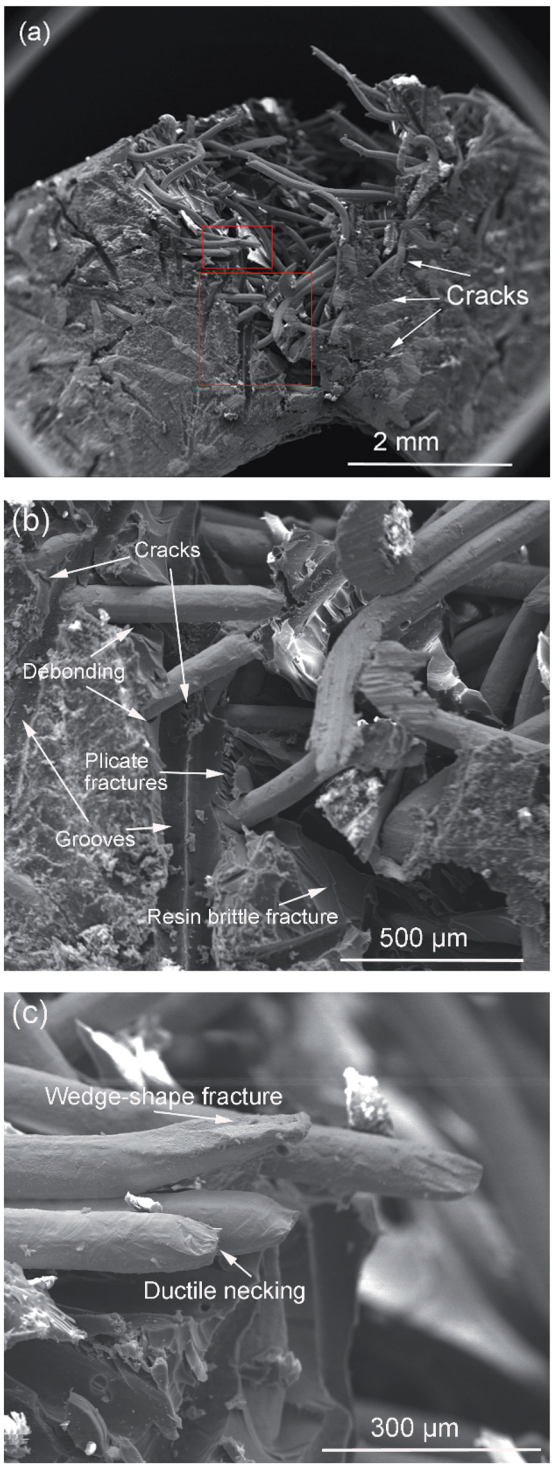

Fig. 8 Fracture morphologies of the IPC with 160 μm fiber diameter and 23.70 vol% fiber fraction in the in-plane direction after bending: (a) lower magnification, (b) and (c) higher magnification.

samples perpendicular to the loading direction because the cracks propagate along the fibers, and fibers fracture in different location. In the IPC with 23.17 vol% fiber fraction, in the through-thickness direction, fiber avulsion happens in the longer length for the different fibrous structure. While for the

IPC with 13.84 vol% fiber fraction, the fracture morphology is similar although serrated cracks exist on the sample surface.

The failure images of the IPC with 160 μm fiber diameter and 23.70 vol% fiber fraction in the in-plane direction are shown in Fig. 8. From Fig. 8a, many cracks can be observed near the fracture surface. From Fig. 8b and c, it is clear that the resin matrix presents typical brittle fracture, *i.e.*, the fracture region is smooth. Certain cracks appear and extend in the resin as relative softer phase deforms plastically first.[35] As there is a large difference of the thermal expansion coefficients between the fibers and the resin, stress concentration is generated in the interface during the manufacturing process, which is the force of crack formation.[30] During the bending process, the tress concentration is serious in the interfaces and corners of the microstructure. With bending progressing, the stress exceeds the interface strength, resulting in the crack formation there.[5,36] Crack propagation is generally limited for the connected structure of the IPC. The failure of the phase with the higher strain improves the fracture resistance by bridging the cracks introduced to the other phase.[31] The IPC after bending deformation shows many sorts of fractures, including cracks in the resin, debonding between fibers and resin, grooves caused by fiber pull-out, plicate fractures caused by extrusion between fibers and smooth resin fracture planes and fiber necking. It is noted that there are different fiber necking characterization. Ductile necking and wedge-shape fracture are observed in the bending process.

Conclusions

(1) Novel metal–resin IPCs are produced by spontaneously infiltrating unsaturated polyester resin into a variety of 304 stainless fiber preforms under vacuum condition and present anisotropic structures, *i.e.*, most fibers distributed in the IPC are parallel to the *x*–*y* plane.

(2) The three-point bending behavior of the IPC presents three stages and anisotropy. The flexural strength and modulus of the IPCs increase with increasing fiber fractions. Nonlinear elastic behavior can be observed in the bending process. Finer fiber can significantly improve the flexural strength and has minor effects on the corresponding displacement. Compared with in-plane direction, the IPCs have higher flexural strength and modulus, and slightly smaller displacement at flexural strength in through-thickness direction. After three-point bending tests, the cracks on the fractured surface along the loading direction are irregular, and the fracture presents serration on the surface of the samples perpendicular to the loading direction. A large difference in fracture appearance in different directions presents after bending, and this difference becomes smaller with decreasing fiber fraction. From the fracture morphologies, IPC after bending deformation shows many sorts of fractures. Plicate and brittle fractures of resin, debonding, fiber pull-out, necking and fracture are the characteristics of the IPC fracture.

Conflicts of interest

There are no conflicts to declare.

Acknowledgements

The project was financially supported by the Science and Technology Program of Guangzhou, China (No. 201604016015) and Special Project of National Development and Reform Commission (ChinaGrid 2011636). Bibo Yao gratefully acknowledges the support from the Chinese Scholarship Council (CSC) and the Doctorate Dissertation Innovation Funds supported by South China University of Technology.

Notes and references

1 R. Jhaver and H. Tippur, *Mater. Sci. Eng., A*, 2009, **499**, 507–517.
2 N. Dukhan, N. Rayess and J. Hadley, *Mech. Mater.*, 2010, **42**, 134–141.
3 L. D. Wegner and L. J. Gibson, *Int. J. Mech. Sci.*, 2001, **43**, 1061–1072.
4 F. Cheng, S.-M. Kim, J. N. Reddy and R. K. Abu Al-Rub, *Int. J. Plast.*, 2014, **61**, 94–111.
5 Z. Zhou, B. Yao, L. Duan and J. Qin, *Adv. Eng. Mater.*, 2018, **20**, 1700669.
6 Y. Qiao, N. Fan, Y. Yu and P. Guo, *Mater. Manuf. Process.*, 2015, **31**, 653–656.
7 A. Mattern, B. Huchler, D. Staudenecker, R. Oberacker, A. Nagel and M. J. Hoffmann, *J. Eur. Ceram. Soc.*, 2004, **24**, 3399–3408.
8 M. T. Isa, A. S. Ahmed, B. O. Aderemi, R. M. Taib and I. A. Mohammed-Dabo, *Composites, Part B*, 2013, **52**, 217–223.
9 K. Konopka, A. Boczkowska, K. Batorski, M. Szafran and K. J. Kurzydyowski, *Mater. Lett.*, 2004, **58**, 3857–3862.
10 H. Prielipp, M. Knechtel, N. Claussen, S. K. Streiffer, H. Müllejans, M. Rühle and J. Rödel, *Mater. Sci. Eng., A*, 1995, **197**, 19–30.
11 W. G. Fahrenholtz, D. T. Ellerby and R. E. Loehman, *J. Am. Ceram. Soc.*, 2000, **83**, 1279–1280.
12 T. Etter, J. Kuebler, T. Frey, P. Schulz, J. F. Löffler and P. J. Uggowitzer, *Mater. Sci. Eng., A*, 2004, **386**, 61–67.
13 R. J. Moon, M. Tilbrook, M. Hoffman and A. Neubrand, *J. Am. Ceram. Soc.*, 2005, **88**, 666–674.
14 D. Horvitz, I. Gotman, E. Y. Gutmanas and N. Claussen, *J. Eur. Ceram. Soc.*, 2002, **22**, 947–954.
15 Z. Zhou, B. Yao, L. Duan and J. Qin, *J. Alloy. Compd.*, 2017, **727**, 146–152.
16 L. D. Wegner and L. J. Gibson, *Int. J. Mech. Sci.*, 2000, **42**, 943–964.
17 W.-y. Chiang and D.-m. Chang, *J. Mater. Sci.*, 1997, **32**, 4985–4990.
18 R. K. Jena, C. Y. Yue, M. M. Sk and K. Ghosh, *RSC Adv.*, 2015, **5**, 79888–79897.
19 O. Al-Ketan, M. Adel Assad and R. K. Abu Al-Rub, *Compos. Struct.*, 2017, **176**, 9–19.
20 M. K. Aghajanian, M. A. Rocazella, J. T. Burke and S. D. Keck, *J. Mater. Sci.*, 1991, **26**, 447–454.
21 B. S. Rao and V. Jayaram, *J. Mater. Res.*, 2001, **16**, 2906–2913.

22 S. Yu, J. Liu, Y. Luo and Y. Liu, *Mater. Sci. Eng., A*, 2007, **457**, 325–328.
23 C. Periasamy, R. Jhaver and H. V. Tippur, *Mater. Sci. Eng., A*, 2010, **527**, 2845–2856.
24 S. Kishimoto and N. Shinya, *Mater. Des.*, 2000, **21**, 575–578.
25 Y. Liu and X.-l. Gong, *Trans. Nonferrous Met. Soc. China*, 2006, **16**, s439–s443.
26 K. H. Hsieh, J. S. Tsai and K. W. Chang, *J. Mater. Sci.*, 1991, **26**, 5877–5882.
27 F. Wu, Z. Zhou, B. Yao and Z. Xiao, *Steel Res. Int.*, 2016, **87**, 1534–1542.
28 W. Zhou, Q. Wang, W. Ling, L. He, Y. Tang, F. Wu, J. Liao, K. S. Hui and K. N. Hui, *Mater. Des.*, 2014, **56**, 522–527.
29 G. S. Daehn, B. Starck, L. Xu, K. F. Elfishawy, J. Ringnalda and H. L. Fraser, *Acta Mater.*, 1996, **44**, 249–261.
30 F. Scherm, R. Völkl, A. Neubrand, F. Bosbach and U. Glatzel, *Mater. Sci. Eng., A*, 2010, **527**, 1260–1265.
31 A. Coldea, M. V. Swain and N. Thiel, *Dent. Mater.*, 2013, **29**, 419–426.
32 N. A. Travitzky and A. Shlayen, *Mater. Sci. Eng., A*, 1998, **244**, 154–160.
33 Z. Zhou, L. Duan and F. Wu, *J. Mater. Res.*, 2017, **32**, 2276–2285.
34 V. Vilay, M. Mariatti, R. Mat Taib and M. Todo, *Compos. Sci. Technol.*, 2008, **68**, 631–638.
35 L. D. Wegner and L. J. Gibson, *Int. J. Mech. Sci.*, 2001, **43**, 1771–1791.
36 L. Wang, Q. Fan, G. Li, H. Zhang and F. Wang, *Comput. Mater. Sci.*, 2014, **95**, 408–413.